Neuro-Oncology

28(8), 1999–2013, 2026 | https://doi.org/10.1093/neuonc/noag088 | Advance Access publication April 20, 2026

Prospective biopsy-controlled validation of an AI model for predicting glioblastoma infiltration: Results from the SupraGlio trial

Santiago Cepeda, Elena Hernando-Pérez, Enrique Pérez-Riesgo, Isabel Rodríguez-Valle, Olga Esteban-Sinovas, Ignacio Arrese, María Miguel Lucero-Salaverry, Tomás Zamora, María Ángeles Torres-Nieto, Luigi Tommaso Luppino, Samuel Kuttner, Marek Wodzinski, Trinidad Escudero, Jesús Garzón, Roberto Romero-Oraá, Roberto Hornero, Lucía Núñez, Carlos Villalobos, and Rosario Sarabia

All author affiliations are listed at the end of the article

Corresponding Author: Santiago Cepeda, MD, PhD, Department of Neurosurgery, Río Hortega University Hospital, Dulzaina 2, Valladolid, 47014, Spain (scepedac@saludcastillayleon.es).

For the podcast associated with this article, please visit 'https://soc-neuro-onc.libsyn.com/oauthor-interviews-prospective-biopsy-controlled-validation-of-an-ai-model-for-predicting-glioblastoma-infiltration-results-from-the-supraglio-trial'

Abstract

Background. Glioblastoma recurrence is driven by diffuse microscopic infiltration beyond the contrast-enhancing tumor margin. GlioMap is an open-access AI model predicting voxelwise infiltration and recurrence risk from multiparametric MRI. This prospective study aimed to validate GlioMap's biological accuracy and prognostic relevance through histopathological assessment, transcriptomic profiling, and survival analysis within the SupraGlio trial (NCT05735171).

Methods. Patients with newly diagnosed glioblastoma underwent neuronavigated biopsies targeting AI-predicted high-risk (HRoR) and low-risk of recurrence (LRoR) regions beyond the contrast-enhancing tumor. Histopathological infiltration served as the ground truth, and transcriptomic profiling characterised each region's molecular phenotype. Model performance was evaluated using accuracy and area under the receiver operating characteristic curve (AUC). Survival analyses assessed the prognostic value of postoperative HRoR volume.

Results. Fifty-eight biopsies from 27 patients were analyzed. GlioMap achieved 0.81 accuracy (95% confidence interval [CI], 0.71-0.91) and 0.84 AUC (95% CI, 0.73-0.93) for histologically confirmed infiltration. Transcriptomic analysis of 48 samples from 16 patients revealed progressive upregulation of invasion- and angiogenesis-related genes (CD44, CHI3L1, STAT3, VEGFA) and downregulation of neuronal markers (MBP, GABRA1) from LRoR to HRoR regions and the tumor core, confirming a neural-to-mesenchymal gradient. Postoperative HRoR volume >1.6 cm^3 predicted shorter overall survival ($P = .04$) and progression-free survival ($P = .008$).

Conclusions. To our knowledge, this study provides the first prospective, biopsy-controlled, molecular validation of an AI model for mapping glioblastoma infiltration. By accurately identifying histologically and transcriptionally infiltrated regions, GlioMap offers a biologically grounded imaging biomarker that could guide extended resection and personalized radiotherapy planning, potentially improving tumor control and patient outcomes.

Key Points

- The GlioMap AI model identified glioblastoma-infiltrated tissue with 81% accuracy.
- High-risk of recurrence regions displayed invasion-related transcriptional programs.
- Large postoperative high-risk recurrence volume was associated with shorter survival.

Received December 13, 2025; accepted April 15, 2026.

Graphical Abstract

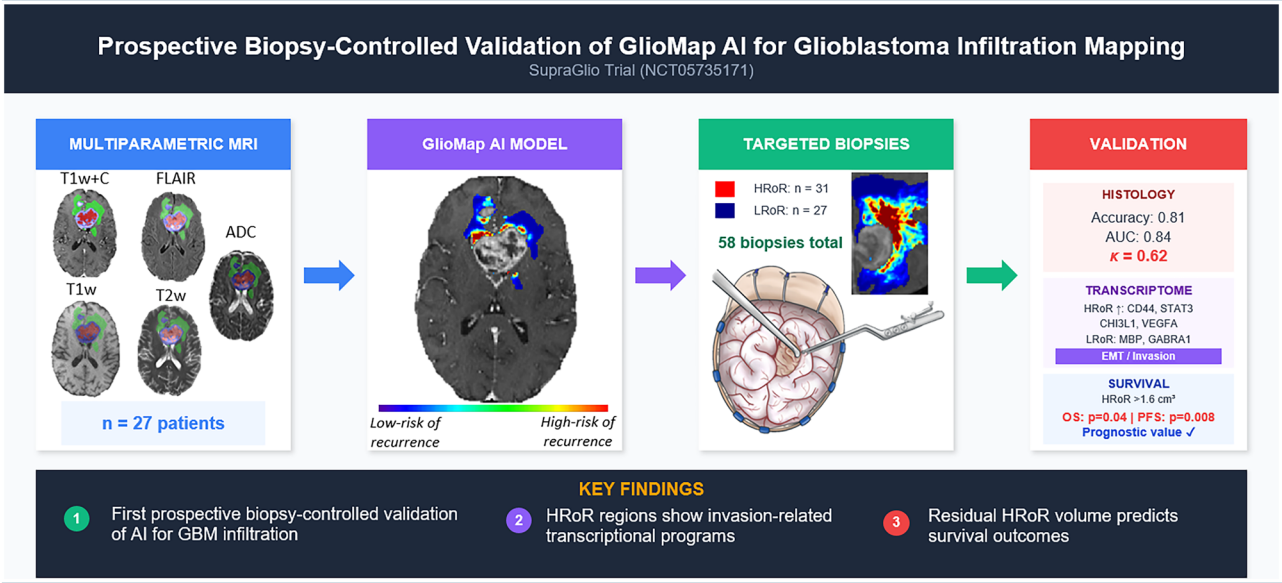

Importance of the Study

Glioblastoma recurrence arises from microscopic invasion beyond contrast-enhanced margins, yet conventional MRI cannot distinguish infiltration from edema. This prospective study provides, to the best of our knowledge, the first histopathological and transcriptomic validation of an AI radiomics model (GlioMap) for identifying infiltrated peritumoral tissue in vivo. By integrating voxelwise MRI features with histopathology and gene expression profiling from neuronavigation-guided biopsies, we demonstrate that AI-predicted high-risk regions harbor malignant transcriptional programs characteristic of invasion, angiogenesis, and epithelial-mesenchymal transition. These findings substantiate the biological validity of radiomics-based infiltration predictions and address a critical limitation of prior imaging studies that lacked synchronous pathological confirmation. Importantly, large residual high-risk volume correlated with shorter progression-free and overall survival, highlighting prognostic and therapeutic relevance. These results support clinical translation of biologically grounded AI maps to guide supramarginal resection and precision radiotherapy dose-painting, potentially reducing marginal recurrences and extending survival in glioblastoma patients.

Despite aggressive multimodal therapy consisting of maximal safe surgical resection, radiotherapy, and chemotherapy, glioblastoma remains among the most lethal malignancies, with a median overall survival (OS) of 12-16 months and a 5-year survival of <10%.[1] Standard surgical planning relies on T1-weighted (T1w) contrast-enhanced MRI to define the gross tumor volume for resection, yet malignant cells routinely infiltrate brain tissue far beyond the contrast-enhanced margins, extending into regions that appear radiologically normal or mildly abnormal on T2-weighted (T2w) and fluid-attenuated inversion recovery (FLAIR) sequences. Histopathology demonstrates infiltration in ~40%-60% of visually normal peritumoral tissue, and up to 90% of recurrences arise at the resection margin despite gross-total resection.[2,3]

This imaging-pathology discrepancy presents a fundamental obstacle to local tumor control.The peritumoral brain zone harbors a unique microenvironment characterized not only by infiltrating tumor cells but also by reactive gliosis, altered vascular permeability, and complex intercellular interactions that are radiologically silent.[4,5] Improved preoperative identification of infiltration-prone regions could enable precision-guided surgical strategies and personalized radiotherapy planning. However, conventional MRI sequences cannot reliably distinguish tumor infiltration from vasogenic edema at the voxel level, limiting the ability of the neurosurgeon to extend resection safely into high-risk peritumoral tissue.[6,7]

Over the past decade, multiparametric MRI and machine learning (ML) have emerged as promising approaches to address this clinical gap. Advanced imaging sequences, including diffusion-weighted imaging, diffusion tensor imaging (DTI), dynamic susceptibility contrast perfusion, and dynamic contrast-enhanced MRI, capture biophysical information about tissue microstructure, cellularity, and haemodynamics that conventional anatomic imaging

cannot provide. Radiomics, the quantitative extraction of texture and shape features from medical images, has been leveraged to construct predictive models that decode imperceptible patterns in these sequences.[8,9]

Leveraging these radiomics features, researchers have developed ML models specifically aimed at predicting the spatial extent of glioblastoma infiltration beyond the contrast-enhancing margin. Early proof-of-concept studies demonstrated that ML models trained on multiparametric MRI could generate voxelwise infiltration probability maps that correlate with postoperative recurrence patterns.[10–15] Landmark studies from single- and multi-institutional cohorts revealed that peritumoral voxels predicted to harbor high infiltration risk were 8-19 times more likely to develop recurrent tumors than those predicting low-risk areas.[16] More recently, deep learning methods have further improved prediction accuracy, achieving cross-validated accuracy in the 85%-93% range and odds ratios of 12.95 in independent validation cohorts.[17]

However, these algorithms face critical limitations that impede clinical translation. A systematic review by Bijlsma et al[18] revealed multiple peer-reviewed studies using voxel-based or region-based AI models, documenting high odds ratios (8.13-19.48) but also substantial variability in sensitivity and specificity across cohorts. Notably, the review emphasized that all published studies relied on indirect validation through postrecurrence imaging rather than pathologically confirmed infiltration at diagnosis. The absence of direct histopathological validation leaves unresolved the fundamental question of whether algorithm-predicted high-risk regions correspond to tumor-infiltrated tissue at the time of diagnosis. As emphasized by the multidisciplinary consensus from the RANO working groups,[19] standardized and spatially guided tissue sampling is essential to capture the biological heterogeneity of diffuse gliomas and to enable reliable clinicopathological correlations. Without adhering to such frameworks, it remains challenging to ascertain whether radiomic or AI-derived high-risk zones truly reflect histologically confirmed tumor infiltration.

To address these clinical needs, an open-access ML model designated GlioMap was developed and made freely available to the scientific and clinical community.[11] GlioMap integrates conventional multiparametric MRI sequences (T1w, T1w contrast-enhanced, T2w, FLAIR, and apparent diffusion coefficient [ADC] maps) using radiomic texture analysis to generate voxelwise probability maps of tumor infiltration and recurrence risk. The model was trained on multi-institutional datasets and validated in external cohorts, and demonstrated robust performance and generalisability across centers.[20]

However, despite the strong external validation of GlioMap through imaging-recurrence correlation, the field recognizes that prospective histopathological validation remains an essential step before GlioMap can be used to guide treatment decision-making with confidence. This requirement mirrors regulatory and clinical expectations for ML deployment: direct evidence that model predictions align with ground-truth pathology is the gold standard.[21,22]

In this context, the SupraGlio-AI trial (NCT05735171) is a prospective study designed to validate GlioMap predictions against histopathologically confirmed tumor infiltration. This trial integrates 3 complementary objectives: (1) independent histological validation of MRI-derived infiltration risk maps using image-guided biopsies; (2) transcriptomic and molecular profiling of infiltrative versus noninfiltrated peritumoral regions to identify biological drivers of radiomics signatures; and (3) in selected patients with noneloquent tumor locations, feasibility, and safety assessment of AI-guided supramarginal resection, extending resection beyond the contrast-enhanced margin into predicted high-risk regions, with evaluation of the extent of resection, perioperative morbidity, and surrogate oncological endpoints.

This framework addresses critical evidence gaps: the lack of synchronous histopathological confirmation at diagnosis, limited understanding of biological heterogeneity underlying radiomics patterns, and the absence of prospective data on AI-guided surgical outcomes. The SupraGlio-AI trial aims to provide evidence for clinical adoption of GlioMap-informed precision treatment and establish standards for histological validation of AI biomarkers in neuro-oncology.

Methods

Study Design and Objectives

The SupraGlio-AI study is a single-center, nonrandomized, prospective clinical trial designed to validate GlioMap, an MRI-based radiomic and ML model that predicts glioblastoma infiltration and recurrence risk within the noncontrast-enhancing peritumoral region. Validation was performed through neuronavigated, image-guided biopsies targeting model-predicted high-risk of recurrence (HRoR) and low-risk of recurrence (LRoR) regions.

The primary objectives were (1) to assess the biological validity of voxelwise model predictions against histopathological findings and (2) to evaluate the feasibility of integrating AI-derived recurrence probability maps into supramarginal resection planning.

The secondary objectives included correlation of HRoR and LRoR regions with transcriptomic and molecular profiles, as well as exploratory analyses of surgical outcomes and survival metrics.

The protocol was approved by the *Comité de Ética de la Investigación con medicamentos* (CEIm) de Valladolid (Ref.: 22-PI208) and conducted in accordance with the Declaration of Helsinki. Written informed consent was obtained from all participants.

This clinical trial was designed and reported in accordance with the SPIRIT-AI[23] and CONSORT-AI[24] guidelines for interventional studies evaluating artificial intelligence systems. The GlioMap model was locked prior to trial initiation, underwent no updates during recruitment, and was applied through a fixed inference pipeline. The reporting of predictive performance follows TRIPOD-AI[25] recommendations, and all imaging acquisition, preprocessing, radiomic extraction, and model integration procedures comply with CLAIM[26] standards for transparency and reproducibility in AI-based imaging research.

Sample Size Justification

Sample size was determined based on infiltration rates reported in prior stereotactic biopsy studies of glioblastoma peritumoral zones, which range from 28% to 89% depending on sampling location.[27,28] Assuming differential infiltration rates between AI-predicted high-risk and low-risk regions, we calculated that 50-60 biopsy specimens would provide adequate statistical power (≥80%, $\alpha = 0.05$) to detect clinically meaningful differences in infiltration rates. The target enrollment of 25-30 patients aligns with sample sizes in comparable prospective validation studies (13-37 patients, 25-60 specimens).[27–29]

Eligibility Criteria

Patients were eligible for inclusion if they presented with a radiological suspicion of supratentorial glioblastoma on preoperative MRI and had a surgical indication with a priori feasibility of gross-total resection, as independently confirmed by 2 senior neurosurgeons. Additional inclusion criteria included a Karnofsky Performance Status (KPS) score ≥70 and the provision of written informed consent.

The exclusion criteria included tumor location within eloquent cortical or subcortical regions precluding safe tissue sampling, recurrent gliomas other than biopsy-only cases, poor-quality MRI studies (eg, due to severe motion or susceptibility artifacts), a KPS score of <60, or severe comorbidities contraindicating surgery (Figure 1).

MRI Acquisition and the GlioMap Pipeline

All patients underwent preoperative multiparametric MRI on a 1.5 T scanner, which included T1w, contrast-enhanced T1w, T2w, FLAIR, and ADC maps. The acquisition protocol details are provided in the Table S1.

The GlioMap workflow included skull stripping, rigid/affine registration of all sequences to a standard atlas space, isotropic resampling, and intensity normalization. The tumor subregions (enhanced core and nonenhanced component) were delineated using the RH-GlioSeg segmentation model.[30] From the nonenhanced FLAIR peritumoral abnormalities, voxelwise radiomic features were extracted across all coregistered sequences.

A CatBoost classifier, trained on >500 000 voxels from 49 subjects across 2 centers using voxelwise radiomic features (first-order statistics and texture descriptors) extracted from the 5 coregistered MRI sequences, with training labels derived from spatial overlap between peritumoral voxels and enhancing tumor on follow-up MRI, and externally validated, generated a per-voxel probability of infiltration and recurrence.[11] Per-voxel probabilities were normalized across the peritumoral region to generate color-coded recurrence probability maps. Areas of HRoR, defined by a predicted probability ≥0.75, were displayed in red, whereas LRoR regions with a probability ≤0.25 were displayed in blue. The color-coded probability maps were fused with the isotropic contrast-enhanced T1-weighted MRI sequence and transferred to the neuronavigation and surgical planning workstation. Predefined target coordinates corresponding to the HRoR and LRoR regions were loaded for intraoperative localization. Image registration and guidance were performed using the Brainlab Curve Navigation System (Brainlab AG, Munich, Germany) (Figure 2).

Intraoperative Workflow and Targeted Biopsy Protocol

To minimize intraoperative brain shift, patient positioning and craniotomy planning were individualized according to tumor location and surgical trajectory to ensure accurate targeting. Surgical navigation was guided by preoperative MRI, intraoperative ultrasound, and 5-ALA fluorescence. In glioblastoma cases suitable for targeted sampling, at least 3 biopsies were obtained per patient: one from the enhanced tumor core and 2 from peritumoral regions corresponding to the HRoR and LRoR zones, located immediately beyond the enhanced tumor margin, as indicated by the GlioMap model (Figure 3). Each peritumoral specimen, approximately 5-10 mm^3 in volume, was divided for histopathological and transcriptomic analyses. In selected cases, AI-guided supramarginal resection was performed when HRoR regions could be safely excised without functional compromise (see Supplementary Methods).

Histopathologic Assessment

All the samples were reviewed by a senior neuropathologist (≥30 years of experience) who was blinded to the imaging-based predictions. Formalin-fixed, paraffin-embedded tissue sections (4 µm) were stained with haematoxylin and eosin (H&E; Sigma-Aldrich) using an automated stainer (Leica ST5020) according to standardized institutional protocols. Immunohistochemical staining for Ki-67 (clone MIB-1, Dako/Agilent; 1:200 dilution) was performed on a Benchmark Ultra platform (Ventana Medical Systems) with antigen retrieval (pH 9.0, 20 min) and DAB chromogen detection. Infiltrated tissue was defined by ≥3 of the following criteria: (1) increased cellularity relative to normal parenchyma, (2) nuclear atypia (hyperchromatic, pleomorphic nuclei), (3) Ki-67 ≥ 3% (≥500 cells counted), (4) ≥1 mitotic figure per 10 high-power fields (×400), (5) microvascular proliferation, or (6) loss of normal architecture. Noninfiltrated tissue showed preserved architecture with ≤1 criterion, representing edema or reactive changes. Any discrepant or diagnostically challenging cases were resolved by consensus between 2 neuropathologists.

RNA Processing and Transcriptomic Analysis

For a selected subset of patients, 3 spatially defined samples were collected per case: enhanced tumor core, HRoR, and LRoR regions as defined by the GlioMap model. All samples were anonymized and processed in a blinded manner during laboratory and computational stages.

Immediately after resection, tissue samples were transported on ice and microdissected (~1 mm^3). RNA was

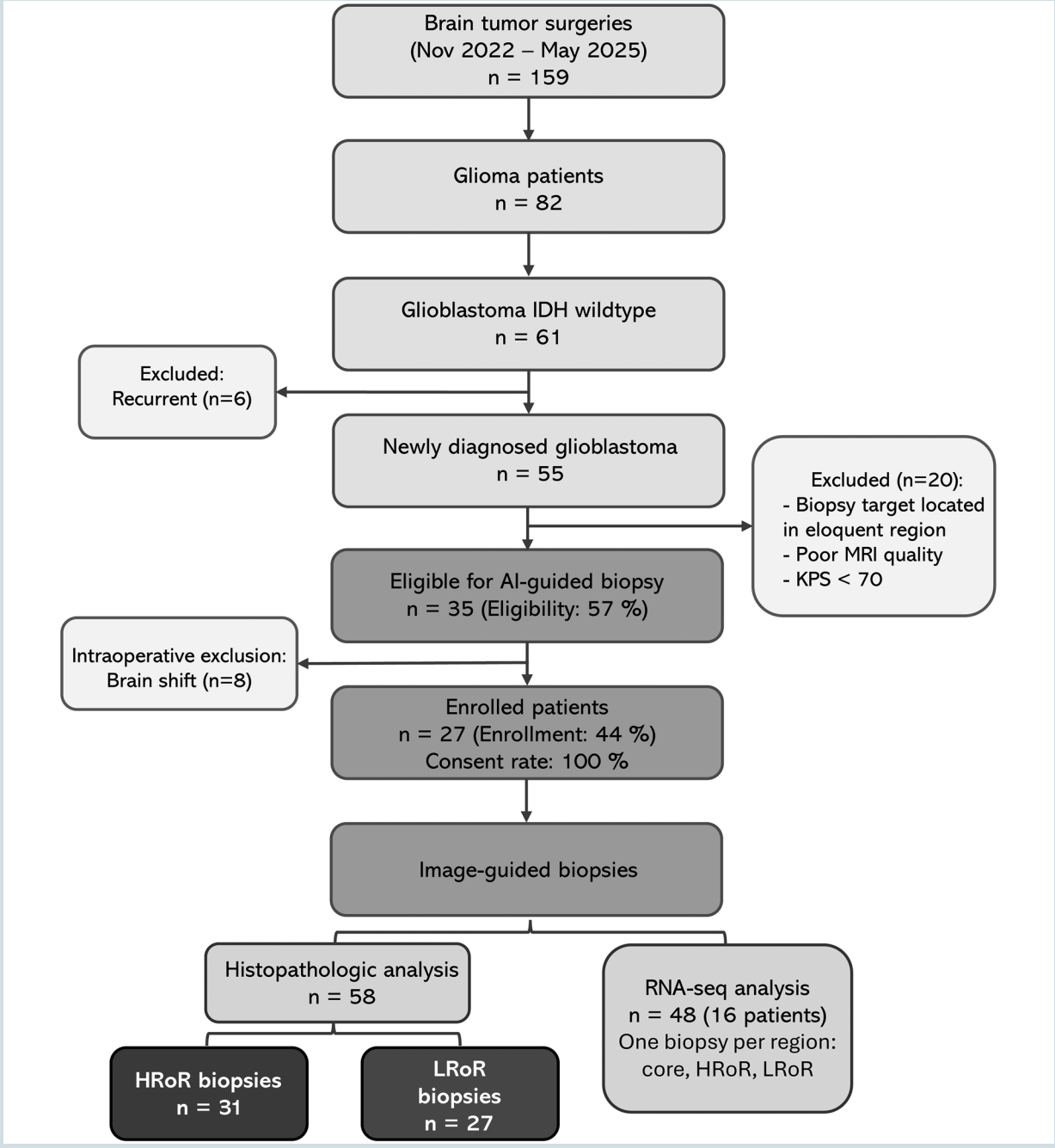

Figure 1. Patient enrollment flowchart. From 159 brain tumor surgeries, 27 patients with newly diagnosed IDH-wild-type glioblastoma were enrolled for AI-guided biopsy. Fifty-eight biopsies underwent histopathologic analysis, and 48 samples from 16 patients were analyzed by RNA sequencing.

extracted using TRIzol-based protocols with DNase treatment, quantified, and quality assessed (RIN ≥ 4). Stranded total RNA libraries with rRNA depletion were prepared from 500 ng of RNA and sequenced on an Illumina NovaSeq 6000 platform (2 × 100 bp), yielding a mean depth of 65 ± 12 million reads per sample, with 93.9% of bases at Q30 or higher.

Raw reads underwent quality control and trimming, followed by 2-pass alignment to the GRCh38 reference genome. Gene-level counts were generated in R, retaining genes with counts per million (CPM) > 1 in at least 3 samples. Differential expression was assessed using voom-limma with patient-level blocking and false discovery rate (FDR) < 0.05.

Gene set enrichment analysis was performed using camera across KEGG, Gene Ontology, and MSigDB collections, focusing on invasion, microenvironmental, and immune-related pathways. Raw and processed data will be deposited in GEO (accession pending), and scripts are available upon request (see Supplementary Methods).

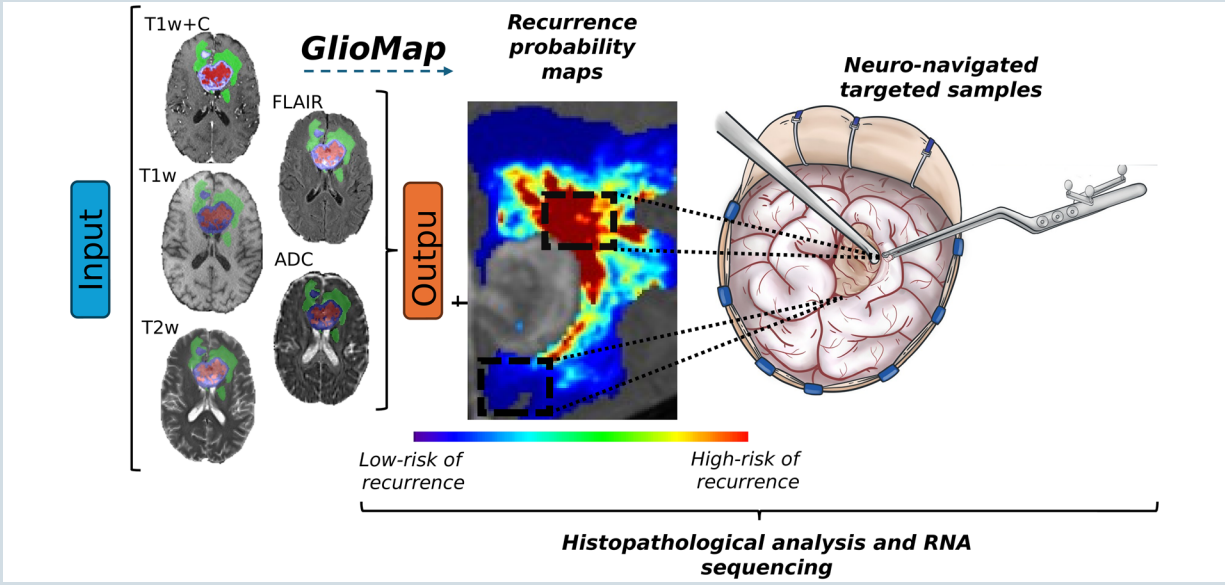

Figure 2. Study workflow for prospective validation of AI-predicted glioblastoma infiltration. Multiparametric MRI sequences (T1-weighted post-contrast [T1w+C], FLAIR, T1-weighted [T1w], apparent diffusion coefficient [ADC], and T2-weighted [T2w]) with automatic tumor segmentation are processed by GlioMap, a machine learning-based model that generates voxelwise recurrence probability maps. Color-coded overlays indicate high-risk of recurrence region (HRoR, red), and low-risk of recurrence region (LRoR, blue). During surgery, neuronavigation-guided targeted biopsies were obtained from each region stratified by AI-predicted infiltration probability. All samples underwent histological analysis and RNA sequencing for molecular characterization and validation of AI predictions.

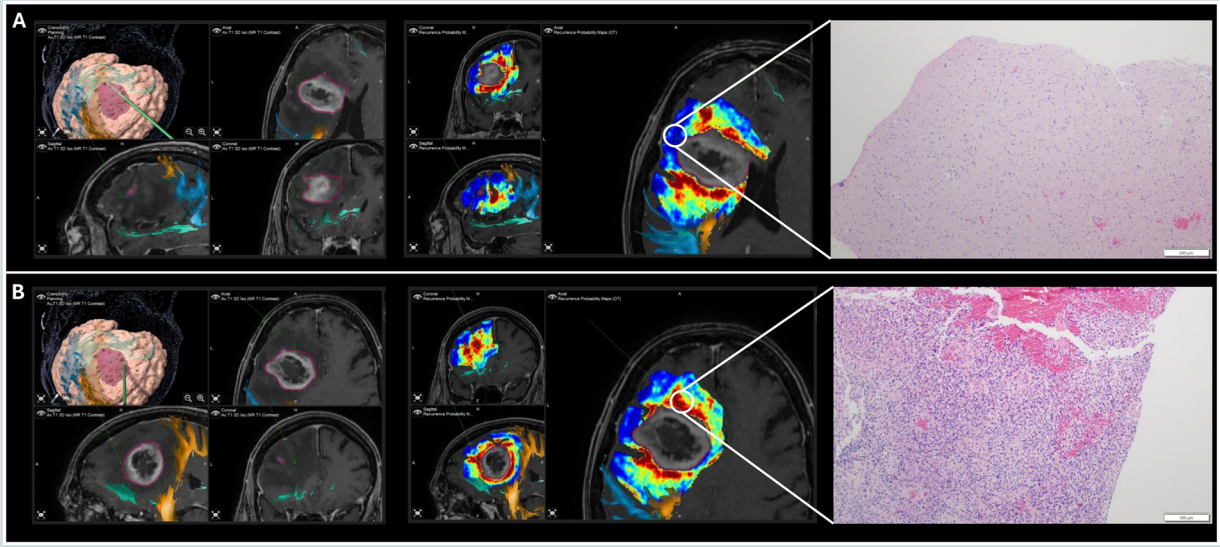

Figure 3. (A) Intraoperative neuronavigation screenshots from a representative case. From left to right: three-dimensional surgical planning view with the navigation pointer shown in green; corresponding T1-weighted contrast-enhanced images; fused recurrence probability maps overlaid on T1w+C, where red denotes high-risk-of-recurrence regions and blue indicates low-risk areas; and the matched H&E histologic section demonstrating normal-appearing white matter. (B) Equivalent sequence of navigation screenshots for a biopsy obtained from a high-risk-of-recurrence region, followed by the corresponding H&E section demonstrating tumor infiltration. In both panels, biopsies were taken immediately outside the contrast-enhanced tumor margin.

Outcome Measurement and Feasibility Analysis

The primary endpoints were feasibility, defined by patient eligibility, consent, and enrollment rates, and the accuracy of the AI model in identifying histologically confirmed infiltrated regions. Feasibility was quantified by calculating the proportion of screened patients fulfilling the inclusion criteria (eligibility rate), those providing written informed consent among the eligible population (consent rate), and those

ultimately enrolled in the AI-guided biopsy protocol (enrollment rate).

Secondary endpoints included OS, defined as the time from surgery to death from any cause or last follow-up, and progression-free survival (PFS), defined as the time from surgery to radiological or clinical progression according to modified RANO criteria.[31] The postoperative volume of the HRoR region was quantified on early postoperative MRI using GlioMap. Patients were then stratified into low- and high-risk categories based on HRoR region volume threshold of 1.6 cm^3, which was previously established in a multicentre retrospective study.[32]

Statistical Analysis

Voxelwise model performance was evaluated using the histopathological infiltration label as the reference standard. The classification metrics included accuracy, sensitivity, specificity, precision, F1 score, balanced accuracy, the Matthews correlation coefficient (MCC), and Cohen's kappa, each with 95% confidence intervals (CIs) estimated by nonparametric bootstrapping (1,000 resamples). Discrimination was quantified by the area under the receiver operating characteristic curve (AUC), with 95% CIs computed using the DeLong method. The McNemar test was applied to assess discordant prediction pairs, and an exact binomial test was used to verify whether the observed accuracy exceeded the 0.5 probability expected by chance. Survival analyses were restricted to patients who underwent resection and adjuvant therapy, and distributions were estimated using the Kaplan-Meier method and compared with the log-rank test. Univariable Cox proportional hazards models were fitted to evaluate the associations of clinical, volumetric, and AI-derived imaging predictors with OS and PFS; hazard ratios (HRs) with 95% CIs were reported; and *P*-value were derived from the Wald test. All the statistical tests were 2-sided, and $P<.05$ was considered to indicate statistical significance. Analyses were performed in R (version 4.3.2, R Foundation for Statistical Computing, Vienna, Austria).

Results

The AI-Guided Biopsy Protocol Achieved High Feasibility and Patient Acceptance

Between February 2023 and May 2025, 159 brain tumor surgeries were performed at our institution, yielding 82 gliomas and 61 WHO 2021-confirmed glioblastomas (55 newly diagnosed, 6 recurrent). Thirty-five patients met all preoperative inclusion criteria. Intraoperatively, 8 patients were excluded because of intraoperative brain shift compromising neuronavigation accuracy, resulting in 27 enrolled patients. The eligibility rate among screened glioblastoma patients was 57% (35/61) with a final enrollment rate of 44% (27/61). All eligible patients provided written informed consent (100% consent rate).

The enrolled cohort had a mean age of 63.5±9.7 years and comprised 16 males (59.3%) and 11 females (40.7%) patients (Table 1). Tumors were predominantly located in the frontal (44.4%) and temporal (33.3%) lobes, with a median preoperative contrast-enhancing volume of 38.4 cm^3 (IQR 21.2-55.1). These demographic and clinical characteristics were representative of the broader glioblastoma population, and the high consent rate combined with the acceptable enrollment proportion indicates that integrating AI-guided targeted biopsy into the standard surgical workflow is both feasible and acceptable to patients.

Model Predictions Achieved Substantial Agreement with Histopathological Assessment

Across the 27 enrolled patients, 58 image-guided biopsies were obtained from predefined targets, including at least one HRoR site and one LRoR site per case, both located immediately outside the contrast-enhanced tumor margin. Histopathological examination served as the reference standard.

The model achieved an accuracy of 0.81 (95% CI, 0.71-0.91), with a sensitivity of 0.86 (95% CI, 0.72-0.97) and a specificity of 0.77 (95% CI, 0.61-0.92). The precision and F1 score were 0.77 (95% CI, 0.63-0.91) and 0.81 (95% CI, 0.70-0.92), respectively. The MCC was 0.63 (95% CI, 0.42-0.83), and Cohen's kappa was 0.62, indicating substantial interrater agreement between model predictions and expert pathology. Receiver operating characteristic analysis yielded an AUC of 0.81 (95% CI, 0.71-0.91; DeLong method). Neither class imbalance nor discordant pair bias was significant (McNemar's $\chi^2 = 0.36$, $P=.55$). The exact binomial test confirmed that the model's accuracy significantly exceeded chance ($P<.001$), demonstrating genuine discriminative ability rather than random classification (Figure 4C-E).

Postoperative HRoR Volume Predicts PFS and OS

Building on the histopathological validation, we investigated whether the extent of residual high-risk tissue after surgery influences clinical outcomes. We hypothesized that incomplete resection of AI-predicted infiltrative zones would correlate with earlier tumor progression and shorter survival. In the filtered cohort ($n=25$, excluding biopsies and patients without adjuvant therapy), dichotomization according to postoperative HRoR volume (cut-off > 1.6 cm^3) revealed significant survival differences. For OS, the high-risk group ($n=20$) experienced more deaths than the low-risk group did ($n=5$) (log-rank $\chi^2 = 4.3$; $P=.04$), with a median OS of 326 days (IQR 133-402) versus 525 days (IQR 422-732), respectively. The difference was more pronounced for PFS (log-rank $\chi^2 = 7.0$; $P=.008$), with median PFS of 168 days (IQR 68-246) in the high-risk group compared with 424 days (IQR 287-461) in the low-risk group (Figure 4A and B).

Univariable Cox analyses identified several clinical and imaging predictors of survival (Table S3). For OS, higher preoperative KPS was associated with lower risk of death (HR 0.955, 95% CI 0.926-0.985, $P=.0033$). Preoperative contrast-enhanced tumor volume did not reach statistical significance (HR 1.02, 95% CI 0.997-1.04, $P=.105$), whereas preoperative T2/FLAIR peritumoral volume exhibited a weak but significant association (HR 1.01, 95% CI 1.00-1.02,

Table 1. Baseline characteristics of the study cohort ($n=27$)

Variable	Value
Demographics	
Age (mean ± SD)	63.5 ± 9.7 years
Sex, *n* (%)—male/female	16 (59.3)/11 (40.7)
Preoperative KPS, *n* (%)—90/80/70	7 (25.9)/14 (51.9)/6 (22.2)
Tumor characteristics	
Tumor location, *n* (%)	
Frontal/temporal/parietal	12 (44.4)/9 (33.3)/4 (14.8)
Occipital/insula	1 (3.7)/1 (3.7)
Laterality, *n* (%)—right/left/bilateral	16 (59.3)/9 (33.3)/2 (7.4)
Eloquent location, *n* (%)—yes/no	14 (51.9)/13 (48.1)
Multifocal, *n* (%)—no/yes	21 (77.8)/6 (22.2)
Preoperative MRI volumes, cm^3, median (IQR)	
Enhanced tumor	38.4 (21.2-55.1)
Peritumoral FLAIR hyperintensity	96.8 (53.2-126.9)
HRoR region volume	8.7 (3.7-14.2)
Surgical variables	
Extent of resection, *n* (%)	
GTR/STR/NTR/biopsy	21 (77.8)/3 (11.1)/1 (3.7)/2 (7.4)
Neurological deficit, *n* (%)	
None/transient	20 (76.9)/3 (11.5)
Minor persistent/major persistent	2 (7.7)/1 (3.8)
Surgical complications, *n* (%)	
None/infarction/infection	25 (92.6)/1 (3.7)/1 (3.7)
Postoperative MRI volumes	
T2/FLAIR volume/HRoR region volume	45.9 (31.3-61.2)/3.0 (2.0-3.6)
Adjuvant treatment	
Received adjuvant treatment, *n* (%)—yes/no	23 (85.2)/4 (14.8)
Radiotherapy dose, Gy, median (IQR)	60.0 (54.0-60.0)
Second-line chemotherapy, *n* (%)—no/yes	18 (66.7)/9 (33.3)
Outcomes	
Overall survival, days, median (IQR)	352.0 (137.5-450.0)
Status at follow-up, *n* (%)—deceased/alive	18 (66.7)/9 (33.3)
Progression-free survival, days, median (IQR)	243.0 (138.0-359.0)
Tumor progression, *n* (%)—yes/no	21 (77.8)/6 (22.2)

Abbreviations: FLAIR, Fluid-Attenuated Inversion Recovery; GTR, gross-total resection; HRoR, high-risk of recurrence; KPS, Karnofsky Performance Status; NTR, near-total resection; STR, subtotal resection.

$P=.0257$), suggesting that extensive peritumoral abnormality influences outcome. Log-transformed postoperative HRoR volume did not reach statistical significance (HR 2.94, 95% CI 0.91-9.47, $P=.0704$). For PFS, the preoperative KPS remained the most robust predictor (HR 0.952, 95% CI 0.919-0.986, $P=.0065$), while neither preoperative tumor volume nor T2/FLAIR abnormality reached statistical significance. Log-transformed postoperative HRoR volume also did not reach statistical significance (HR 2.13, 95% CI 0.91-4.97, $P=.081$). These findings suggest that AI-identified high-risk regions represent biologically relevant zones of tumor infiltration and that residual disease within these regions contributes to disease progression and mortality (see Figure S1).

Spatially Targeted Samples Reveal Distinct Transcriptional Programs Across Tumor Compartments

Forty-eight spatially annotated samples from 16 glioblastoma patients were analyzed. For each patient, 3 anatomically defined regions were collected according to MRI and AI-derived maps. The initial transcript catalog included 78 932 ENSEMBL-annotated transcripts (hg38). After removing transcripts with zero counts ($n=12\,512$) and applying expression filtering (EdgeR's filterByExpr), 25 834 entries were retained. Exclusion of transcripts without valid gene symbols resulted in 18 917 genes for downstream analysis.

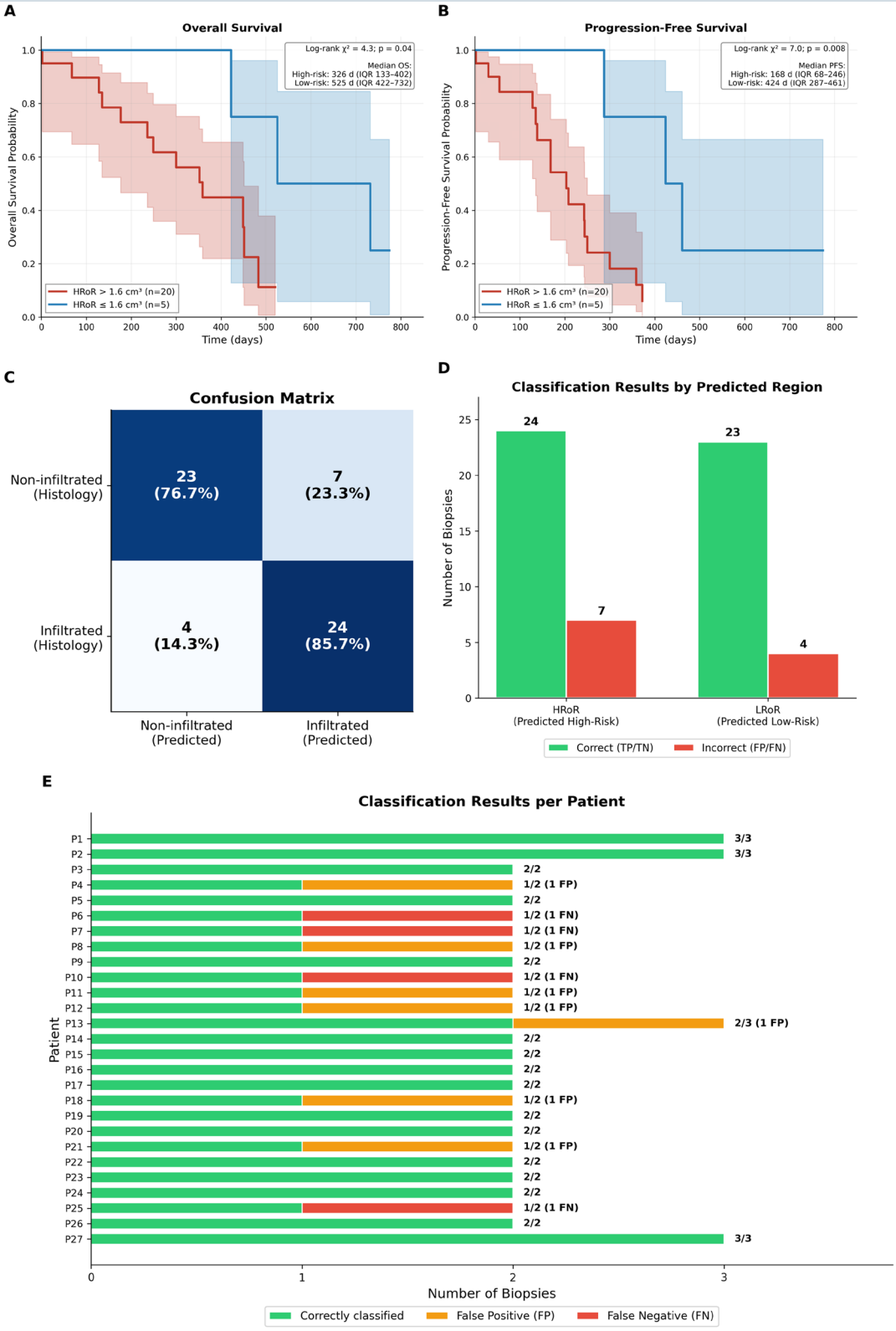

Figure 4. Model performance and survival analyses. Kaplan-Meier curves for overall survival (A), and progression-free survival (B) stratified by postoperative HRoR region volume. (C) Confusion matrix comparing predicted infiltration with histopathological findings. (D) Per-patient classification bars illustrating correct classifications, false-positives, and false-negatives. (E) Bar chart showing the number of correctly and incorrectly classified biopsies across high-risk (HRoR) and low-risk of recurrence (LRoR) regions.

Differential expression analysis (voom-limma with quality weights, robust empirical Bayes moderation, and patient-level blocking) revealed marked transcriptional differences between spatial compartments: tumor core vs. HRoR yielded 5041 differentially expressed genes (DEGs) (27.00%); tumor core vs. LRoR yielded 9341 DEGs (50.03%); and HRoR vs. LRoR yielded 2609 DEGs (13.97%). Canonical glioblastoma-related genes exhibited expected expression patterns. In the tumor core vs. LRoR comparison, CHI3L1, CD44, VEGFA, CA9, HIF1A, SOX2, STAT3, NRAS, MAPK7, MAPK12, AKT1, NFKB2, and TGFB2 were up-regulated, whereas neuronal and oligodendroglial markers including ALDH1A3, PIK3CB, GABRA1, SYT1, MBP, PLP1, EGLN3, HRAS, MAPK3, MAPK4, MAPK9, and MAPK10 were down-regulated (Table S2). In the tumor core vs. HRoR contrast, many alterations persisted (eg, VEGFA, CA9, SOX2, MAPK7, MAPK12, AKT1, MAPK3, PIK3CB, MBP, PLP1), while invasion-related genes such as MERTK and AXL displayed context-dependent regulation at the invasive front. Two PIK3 catalytic subunits, PIK3CG and PIK3CD, were down-regulated. In the HRoR vs. LRoR comparison, several glioblastoma-associated transcripts (VEGFA, HIF1A, STAT3, CD44, NRAS, MAPK7, AKT1) were up-regulated, whereas MAPK9, MAPK10, and neuronal markers such as GABRA1 (FDR = 0.06) were down-regulated (Figure 5). These expression patterns indicate that the peritumoral high-risk tissue already harbors a transcriptional profile consistent with early tumor infiltration, supporting the biological validity of the AI model's predictions (Figure S2).

HRoR Regions Exhibit Enrichment for Invasion and Mesenchymal Transition Programs

To further characterize the functional programs distinguishing AI-predicted high-risk zones from low-risk peritumoral tissue, we performed competitive gene set enrichment analysis across comprehensive pathway databases. This analysis aimed to identify coordinated transcriptional programs underlying tumor invasion and to determine whether the HRoR compartment represents a transitional state between the tumor core and normal brain. Competitive gene set analysis (camera) was performed across 34 837 MSigDB gene sets while accounting for inter-gene correlation. Significant pathway enrichment (FDR < 0.05) was identified for 2946 sets in the tumor core vs. HRoR comparison, 2643 in the tumor core vs. LRoR, and 8111 in the HRoR vs. LRoR. Enriched programs included hallmark oncogenic pathways, glioblastoma subtype signatures, and processes related to invasion and microenvironmental remodeling.

The HRoR vs. LRoR contrast exhibited the most coherent enrichment profile, dominated by epithelial-mesenchymal transition, TGF-β signaling, angiogenesis, inflammatory and interferon responses, and cellular plasticity. Notable enriched glioblastoma-associated signatures included VERHAAK_GLIOBLASTOMA_MESENCHYMAL and VERHAAK_GLIOBLASTOMA_NEURAL, along with invasion-related metaprograms such as ANASTASSIOU_MULTICANCER_INVASIVENESS_SIGNATURE and SOTIRIOU_BREAST_CANCER_GRADE_1_VS_3_UP. In contrast, the tumor core vs. LRoR comparison yielded the greatest number of DEGs but fewer coherent enrichments,

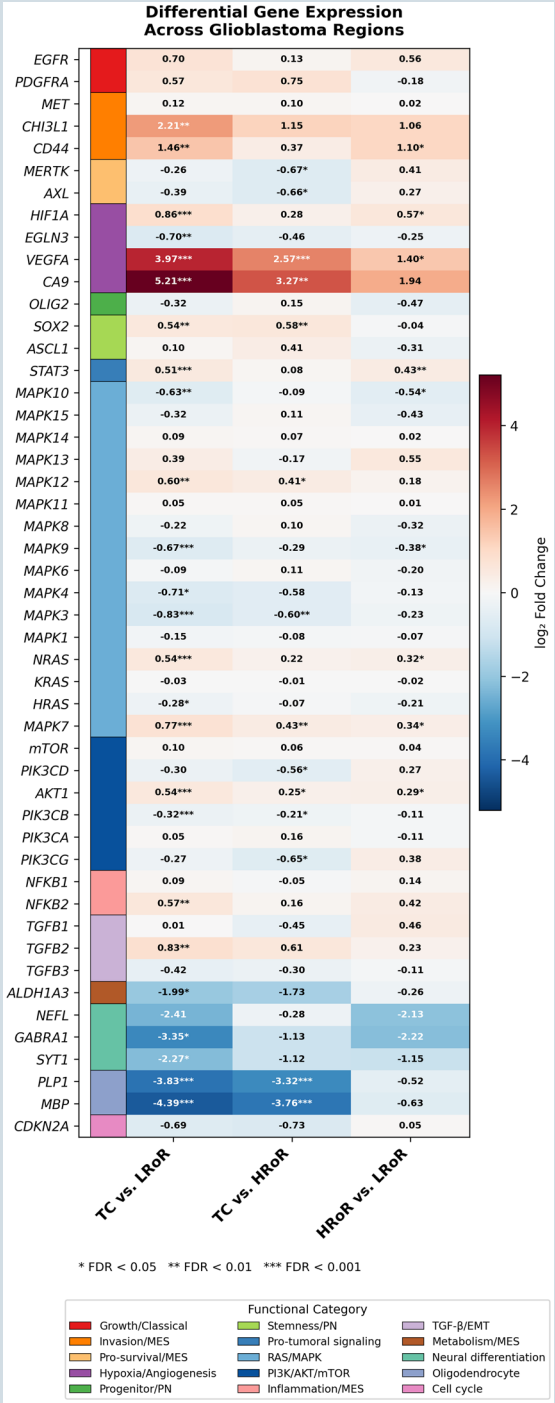

Figure 5. Differential gene expression across tumor core (TC), high-risk of recurrence (HRoR), and low-risk of recurrence (LRoR) regions. Heatmap showing $\log_2$ fold-change values for selected glioblastoma-related genes across 3 pairwise comparisons (TC vs. LRoR, TC vs. HRoR, and HRoR vs. LRoR). Genes are grouped by functional category, indicated by the color bar on the left. Warm colors represent upregulation and cool colors downregulation. Asterisks denote statistical significance after FDR correction (*FDR < 0.05; **FDR < 0.01; ***FDR < 0.001).

consistent with the heterogeneous cellular composition of the core (coexisting proliferative, hypoxic, and necrotic zones). The tumor core vs. HRoR contrast showed an intermediate profile, sharing neural identity and cell cycle-related programs with HRoR vs. LRoR, suggesting that the peritumoral high-risk region partially recapitulates transcriptional programs of the tumor at lower amplitude. These enrichment patterns demonstrate that AI-identified high-risk zones are characterized by the coordinated activation of invasion and mesenchymal programs, providing molecular evidence that these regions represent genuine infiltrative fronts rather than passive edema or normal tissue (Figures S3 and S4).

Discussion

GlioMap achieved high discriminative performance (accuracy = 0.81; AUC = 0.81) in differentiating infiltrated from noninfiltrated peritumoral tissue using routine MRI, with substantial histopathological agreement (Cohen's $\kappa = 0.62$). Clinical integration proved feasible, with 44% eligibility and 100% consent rates. Transcriptomic analysis of 48 samples from 16 patients revealed that high-risk regions harbor coordinated molecular programs of early infiltration, including epithelial-mesenchymal transition, angiogenesis, and immune modulation, establishing biological validity for radiomic predictions. Residual postoperative high-risk volume correlated with progression-free and OS. These findings establish GlioMap as a biologically validated tool bridging radiomic predictions, histopathology, and molecular phenotypes for mapping glioblastoma infiltration.

Comparison With Previous Biopsy-Validated Imaging and AI Approaches

Previous MRI-histology studies established correlations between imaging abnormalities and tumor cellularity but lacked predictive or molecular validation. Durst et al,[33] Chang et al,[34] and Eidel et al[28] confirmed that diffusion, perfusion, and FLAIR abnormalities extend beyond enhancement; nearly 90% of nonenhanced samples contained tumor cells. However, these cross-sectional studies described only associations ($r \approx 0.74$) and lacked integration with molecular phenotypes. Mechanistic and learning-based models by Gaw et al[35] and Hu et al[36] simulated proliferation-invasion dynamics and estimated cell density ($r = 0.84$) but relied on theoretical priors rather than histological ground truth.

More recently, AI models have predicted recurrence patterns[10,12–15,37,38] with impressive accuracy but lacked synchronous histopathological evidence to validate that predicted high-risk zones actually contained tumor cells at the time of surgery. Deep learning and radiopathomic frameworks[27,29] advanced voxelwise detection using DTI or conventional MRI, achieving an AUC of 0.93 and a specificity of 0.89; however, sensitivity remained limited (typically <0.70), and sample sizes were small ($n < 30$ biopsies). Autopsy-based radiopathomic studies[39–41] confirmed tumor spread up to 10 cm beyond enhancement but were affected by postmortem tissue distortion and loss of microenvironmental fidelity, including collapse of vasculature and altered cellularity.

Unlike prior imaging or radiopathomic approaches, GlioMap operates entirely on routine clinical MRI without advanced acquisitions or postmortem data. By demonstrating that AI-predicted high-risk regions harbor coordinated upregulation and invasion-associated pathways, our study provides the missing biological link between imaging features and molecular phenotype. This multidimensional validation represents a conceptual shift from estimating cell density to identifying functionally malignant tissue, redefining how glioblastoma infiltration can be mapped and targeted in vivo.

Biological Validation: Transcriptomic Analysis Across AI-Defined Regions

Spatial RNA sequencing across 48 samples from 16 patients revealed a continuous molecular gradient from the enhanced core to the peritumoral brain, supporting the hypothesis that glioblastoma infiltration is not a binary phenomenon but rather a spatially graded transition.[42,43] Differential expression analysis identified 9341 DEGs between the tumor core and LRoR, 5041 between the core and HRoR, and 2609 between the HRoR and LRoR. Notably, the HRoR-LRoR contrast exhibited the most coherent enrichment pattern, suggesting that this comparison best captures the molecular transition from infiltrated to uninvolved tissue.

The HRoR region exhibited progressive upregulation of invasion and stem-cell markers including CD44, CHI3L1 (YKL-40), SERPINA3, STAT3, VEGFA, and SOX2, alongside downregulation of neuronal markers (GABRA1, MBP, PLP1), indicating a shift toward extracellular matrix remodeling, angiogenesis, and cellular plasticity. CD44 is a marker of invasiveness and stemness,[44] SERPINA3 contributes to EMT and radioresistance,[45] and CHI3L1 promotes angiogenesis and immune evasion.[46] Gene set enrichment confirmed dominant pathways involving TGF-β, IL6-JAK-STAT3, NF-κB, angiogenesis, hypoxia, and EMT, canonical hallmarks of infiltrative glioblastoma.[7,43] Immune profiling indicated macrophage polarization and exhaustion signatures,[4,47] suggesting that HRoR regions not only harbor malignant cells but also exhibit immunosuppressive microenvironments that may facilitate invasion and therapeutic resistance.

Conversely, the LRoR region preserved neuronal and oligodendroglial signatures (SYT1, GABRA1, MBP, PLP1), confirming spatial specificity and demonstrating that the AI model successfully distinguishes infiltrated from uninvolved peritumoral tissue. This neural-to-mesenchymal continuum integrates transcriptional plasticity and immune modulation into a unified invasion framework, providing mechanistic insight into the biology encoded by radiomic features. The integration of radiomics, histopathology, and spatial transcriptomics establishes a biologically grounded paradigm for infiltration mapping and highlights targetable molecular pathways (CD44, SERPINA3, STAT3, VEGFA) for precision therapy in future clinical trials.

Clinical and Prognostic Implications

The biological validation of AI-predicted infiltration zones raises the critical question of whether these regions have clinical relevance for patient outcomes. Our survival analysis provides evidence that residual HRoR volume after surgery functions as an independent prognostic factor. Patients with an unresected HRoR volume >1.6 cm^3 exhibited significantly shorter PFS (median 168 vs. 424 days, P=.008) and OS (median 326 vs. 525 days, P=.04), underscoring the clinical relevance of this compartment. These findings suggest that AI-identified high-risk regions represent biologically active disease that contributes to recurrence and mortality when left unresected.

From a therapeutic perspective, voxelwise infiltration probabilities might enable biologically individualized radiotherapy planning, allowing dose escalation to the highest-risk areas while sparing uninvolved brain. This approach aligns with computational models by Balcerak et al[48] and Lipková et al,[49] which demonstrate that integrating patient-specific infiltration maps into dose-painting protocols improves coverage of recurrence-prone regions without increasing total radiation volume.

Limitations and Interpretation of Findings

This study has several limitations that inform interpretation of the results and highlight priorities for future research. First, as a single-center study with 27 enrolled patients and 16 patients included in transcriptomic analysis, the cohort size may limit generalizability. The 44% enrollment rate reflects biopsy safety requirements, whereas GlioMap can generate predictions for any glioblastoma with standard MRI. Although GlioMap was trained on multicentre data,[11,20] external histopathological and molecular validation across diverse scanners, imaging protocols, and patient populations is essential to establish robustness.

Second, intraoperative brain shift, although minimized with ultrasound-guided correction, may introduce minor spatial localization errors (typically 2-3 mm) that could affect biopsy-to-prediction correspondence. This technical limitation, inherent to all neuronavigation-based studies, may contribute to instances where histologically negative biopsies arise from AI-predicted high-risk zones or vice versa.

Third, the HRoR and LRoR thresholds (≥0.75 and ≤0.25, respectively) were set a priori based on modeling assumptions and may benefit from adaptive, patient-specific calibration. Optimal threshold selection could be refined through receiver operating characteristic analysis in larger cohorts or through integration with clinical endpoints.

Finally, the transcriptomic analysis was limited to 16 patients due to the resource-intensive nature of RNA sequencing and may not fully capture the molecular heterogeneity of glioblastoma. Key molecular features such as MGMT promoter methylation status, EGFR amplification, or TERT promoter mutations were not systematically integrated into the radiogenomic analysis, yet these features are known to influence infiltration patterns and treatment response. Larger studies incorporating comprehensive molecular profiling, including whole-exome sequencing, methylation arrays, and single-cell transcriptomics, are needed to determine whether specific molecular subtypes exhibit distinct radiomic signatures and whether model performance varies by genetic background.

Future Directions and Implications for Research

The findings of this study open multiple avenues for clinical translation and basic research. From a clinical perspective, future research should pursue multicentre, multivendor validation under harmonized imaging protocols to meet regulatory standards and achieve CE-marking or FDA approval. Prospective trials comparing AI-guided supramarginal resection to standard resection, with endpoints including survival, quality of life, and neurocognitive outcomes, are critical to establish clinical utility. Integration of GlioMap into commercial surgical navigation platforms and radiotherapy planning systems would enable real-time, biology-guided decision-making during surgery and treatment planning.

Building on these clinical priorities, our group has launched the ARTPLAN-GLIO trial (Artificial Intelligence-Guided Radiotherapy Planning for Glioblastoma, NCT06657027), a prospective study testing biologically individualized radiotherapy guided by AI-derived infiltration maps. This trial will assess whether dose escalation to AI-predicted high-risk zones improves local control without increasing toxicity, directly addressing the clinical relevance of radiomic infiltration mapping.

Furthermore, the molecular pathways identified in HRoR regions, particularly EMT, STAT3, VEGFA, and immune modulation, represent targetable vulnerabilities that could be exploited therapeutically. Basic researchers could use AI-predicted infiltration maps to guide preclinical studies, enriching animal models or organoid systems with cells harvested from radiomically defined compartments. This approach could accelerate the discovery of infiltration-specific therapeutic targets and enable the testing of spatially targeted drug delivery strategies.

Finally, our findings confirm that the peritumoral zone comprises spatially distinct molecular microenvironments. Future research should investigate how these gradients influence cellular plasticity, immune surveillance, and treatment response. Spatial proteomics, metabolomics, and multiplex immunohistochemistry could complement transcriptomics to build molecular atlases of the tumor-brain interface. The convergence of AI, advanced imaging, spatial omics, and molecular pathology heralds a paradigm shift from anatomically defined to biologically personalized neuro-oncologic care.

Supplementary Material

Supplementary material is available online at *Neuro-Oncology* (https://academic.oup.com/neuro-oncology).

Keywords

artificial intelligence | glioblastoma | infiltration | radiomics | recurrence

Author Contributions

Conceptualization: S.C.; Methodology: S.C., E.H.-P., and E.P.-R.; Software: S.C., L.T.L., S.K., M.W., and R.R.; Validation: S.C., E.H.-P., and E.P.-R.; Formal analysis: S.C., E.H.-P., and E.P.-R.; Investigation: S.C., O.E.-S., and I.A.; Resources: S.C.; Data curation: S.C., T.E., and J.G.; Writing—original draft: S.C. and E.P.-R.; Writing—review & editing: all authors; Visualization: S.C. and E.P.-R.; Supervision: S.C., R.H., C.V., and L.N.; Project administration: S.C.; Funding acquisition: S.C.

Conflict of Interest Statement

The GlioMap algorithm has been formally disclosed through a Disclosure of Invention (DOFI) filed with the University Hospital of Northern Norway (UNN), reference DOFI 2024/8833. The authors report no financial interests or royalties associated with this disclosure.

Funding

This work was supported by the Instituto de Salud Carlos III (ISCIII), Proyectos I+D+i, Acción Estratégica en Salud 2022 [grant number PI22/01680]. Additional support was provided by the European Union's Recovery and Resilience Facility—NextGenerationEU, within the framework of the Spanish Government's public business entity Red.es call for participation in talent attraction and retention programs, under Investment 4 of Component 19 of the Recovery, Transformation and Resilience Plan.

Ethical Approval

This prospective clinical trial was approved by the Comité de Ética de la Investigación con medicamentos (CEIm) de Valladolid (Ref.: 22-PI208) and conducted in accordance with the Declaration of Helsinki and all applicable regulatory standards. Written informed consent was obtained from all participants prior to enrollment.

Data Availability

The voxelwise infiltration model (GlioMap) and the deep learning-based segmentation model (RH-GlioSeg) are freely accessible through the GEIBAC research platform: https://geibac.uva.es/.

Affiliations

Department of Neurosurgery, Río Hortega University Hospital, Valladolid, Spain (S.C., O.E.-S., I.A., R.S.); Specialized Group in Biomedical Imaging and Computational Analysis (GEIBAC), Instituto de Investigación Biosanitaria de Valladolid (IBioVALL), Valladolid, Spain (S.C., O.E.-S., I.A., R.S.); Excellence Unit Institute of Biomedicine and Molecular Genetics of Valladolid (IBGM), University of Valladolid and Spanish National Research Council (CSIC), Valladolid, Spain (E.H.-P., E.P.-R., I.R.-V., L.N., C.V.); Department of Cell Biology, Histology and Pharmacology, School of Medicine, University of Valladolid, Valladolid, Spain (E.H.-P.); Health Sciences School, Miguel de Cervantes European University (UEMC), Valladolid, Spain (E.H.-P.); Department of Pathology, Río Hortega University Hospital, Valladolid, Spain (M.M.L.-S., T.Z., M.Á.T.-N.); Norwegian Computing Center (Norsk Regnesentral), Oslo, Norway (L.T.L.); PET Imaging Center, University Hospital of North Norway, Tromsø, Norway (S.K.); UiT Machine Learning Group, UiT The Arctic University of Norway, Tromsø, Norway (S.K.); Department of Measurement and Electronics, AGH University, Kraków, Poland (M.W.); Sano Centre for Computational Medicine, Kraków, Poland (M.W.); Department of Radiology, Río Hortega University Hospital, Valladolid, Spain (T.E., J.G.); Biomedical Engineering Group, University of Valladolid, Instituto de Investigación Biosanitaria de Valladolid (IBioVALL), Valladolid, Spain (R.R.-O., R.H.); Center for Biomedical Research in Network of Bioengineering, Biomaterials and Nanomedicine (CIBER-BBN), Valladolid, Spain (R.R.-O., R.H.); Institute for Research in Mathematics (IMUVA), University of Valladolid, Valladolid, Spain (R.H.); Department of Biochemistry and Molecular Biology and Physiology, School of Medicine, University of Valladolid, Valladolid, Spain (L.N.)

References

1. Koshy M, Villano JL, Dolecek TA, et al. Improved survival time trends for glioblastoma using the SEER 17 population-based registries. *J Neurooncol*. 2012;107:207-212. https://doi.org/10.1007/s11060-011-0738-7
2. Lemée JM, Clavreul A, Menei P. Intratumoral heterogeneity in glioblastoma: don't forget the peritumoral brain zone. *Neuro Oncol*. 2015;17:1322-1332. https://doi.org/10.1093/neuonc/nov119
3. Petrecca K, Guiot MC, Panet-Raymond V, Souhami L. Failure pattern following complete resection plus radiotherapy and temozolomide is at the resection margin in patients with glioblastoma. *J Neurooncol*. 2013;111:19-23. https://doi.org/10.1007/s11060-012-0983-4
4. Rahimi Koshkaki H, Minasi S, Ugolini A, et al. Immunohistochemical characterization of immune infiltrate in tumor microenvironment of glioblastoma. *J Pers Med*. 2020;10:112. https://doi.org/10.3390/jpm10030112
5. Trevisi G, Barbone P, Treglia G, Mattoli MV, Mangiola A. Reliability of intraoperative ultrasound in detecting tumor residual after brain diffuse glioma surgery: a systematic review and meta-analysis. *Neurosurg Rev*. 2020;43:1221-1233. https://doi.org/10.1007/s10143-019-01160-x
6. Giambra M, Di Cristofori A, Valtorta S, et al. The peritumoral brain zone in glioblastoma: where we are and where we are going. *J Neurosci Res*. 2023;101:199-216. https://doi.org/10.1002/jnr.25134
7. Ballestín A, Armocida D, Ribecco V, Seano G. Peritumoral brain zone in glioblastoma: biological, clinical and mechanical features. *Front Immunol*. 2024;15:1347877. https://doi.org/10.3389/fimmu.2024.1347877
8. d'Este SH, Nielsen MB, Hansen AE. Visualizing glioma infiltration by the combination of multimodality imaging and artificial intelligence, a

systematic review of the literature. *Diagnostics*. 2021;11:592. https://doi.org/10.3390/diagnostics11040592

9. Lambin P, Leijenaar RTH, Deist TM, et al. Radiomics: the bridge between medical imaging and personalized medicine. *Nat Rev Clin Oncol*. 2017;14:749-762. https://doi.org/10.1038/nrclinonc.2017.141
10. Akbari H, Macyszyn L, Da X, et al. Imaging surrogates of infiltration obtained via multiparametric imaging pattern analysis predict subsequent location of recurrence of glioblastoma. *Neurosurgery*. 2016;78:572-580. https://doi.org/10.1227/NEU.0000000000001202
11. Cepeda S, Luppino LT, Pérez-Núñez A, et al. Predicting regions of local recurrence in glioblastomas using voxel-based radiomic features of multiparametric postoperative MRI. *Cancers (Basel)*. 2023;15:1894. https://doi.org/10.3390/cancers15061894
12. Chougule T, Gupta RK, Saini J, et al. Radiomics signature for temporal evolution and recurrence patterns of glioblastoma using multimodal magnetic resonance imaging. *NMR Biomed*. 2022;35:e4647. https://doi.org/10.1002/nbm.4647
13. Dasgupta A, Geraghty B, Maralani PJ, et al. Quantitative mapping of individual voxels in the peritumoral region of IDH-wildtype glioblastoma to distinguish between tumor infiltration and edema. *J Neurooncol*. 2021;153:251-261. https://doi.org/10.1007/s11060-021-03762-2
14. Rathore S, Akbari H, Doshi J. Radiomic signature of infiltration in peritumoral edema predicts subsequent recurrence in glioblastoma: implications for personalized radiotherapy planning. *J Med Imag*. 2018;5:1. https://doi.org/10.1117/1.JMI.5.2.021219
15. Yan J-L, Li C, van der Hoorn A, Boonzaier NR, Matys T, Price SJ. A neural network approach to identify the peritumoral invasive areas in glioblastoma patients by using MR radiomics. *Sci Rep*. 2020;10:9748. https://doi.org/10.1038/s41598-020-66691-6
16. Mohan S, Garcia J, Akbari H, et al. Nimg-47. MULTI-institutional validation of an AI-based model for prediction of tumor infiltration and future recurrence in patients with glioblastoma: results from the respond consortium. *Neuro-Oncology*. 2024;26:viii205-viii206. https://doi.org/10.1093/neuonc/noae165.0811
17. Kwak S, Akbari H, Garcia JA, et al. Predicting peritumoral glioblastoma infiltration and subsequent recurrence using deep-learning-based analysis of multi-parametric magnetic resonance imaging. *J Med Imaging (Bellingham)*. 2024;11:054001. https://doi.org/10.1117/1.JMI.11.5.054001
18. Bijlsma S, Maal T, Rubbert C, et al. AI radiomics predicts spatial glioma recurrence on preoperative MRI: a systematic review. *Eur J Radiol*. 2025;193:112412. https://doi.org/10.1016/j.ejrad.2025.112412
19. Karschnia P, Smits M, Reifenberger G, Expert Rater Panel, et al. A framework for standardised tissue sampling and processing during resection of diffuse intracranial glioma: joint recommendations from four RANO groups. *Lancet Oncol*. 2023;24:e438-e450. https://doi.org/10.1016/S1470-2045(23)00453-9
20. Cepeda S, Luppino L, Wodsinski M, et al. Nimg-45. EXTERNAL evaluation of a machine learning model employing radiomics to identify regions of local recurrence in glioblastoma from postoperative mri. *Neuro-Oncology*. 2023;25:v195-v196. https://doi.org/10.1093/neuonc/noad179.0741
21. Bluemke DA, Moy L, Bredella MA, et al. Assessing radiology research on artificial intelligence: a brief guide for authors, reviewers, and Readers-From the radiology editorial board. *Radiology*. 2020;294:487-489. https://doi.org/10.1148/radiol.2019192515
22. Benjamens S, Dhunnoo P, Meskó B. The state of artificial intelligence-based FDA-approved medical devices and algorithms: an online database. *NPJ Digit Med*. 2020;3:118. https://doi.org/10.1038/s41746-020-00324-0
23. Cruz Rivera S, Liu X, Chan AW, SPIRIT-AI and CONSORT-AI Consensus Group, et al. Guidelines for clinical trial protocols for interventions involving artificial intelligence: the SPIRIT-AI extension. *Nat Med*. 2020;26:1351-1363. https://doi.org/10.1038/s41591-020-1037-7
24. Liu X, Rivera SC, Moher D, Calvert MJ, Denniston AK, SPIRIT-AI and CONSORT-AI Working Group Reporting guidelines for clinical trial reports for interventions involving artificial intelligence: the CONSORT-AI extension. *BMJ*. 2020;370:m3164. https://doi.org/10.1136/bmj.m3164
25. Collins GS, Moons KGM, Dhiman P, et al. TRIPOD+AI statement: updated guidance for reporting clinical prediction models that use regression or machine learning methods. *BMJ*. 2024;385:e078378. https://doi.org/10.1136/bmj-2023-078378
26. Mongan J, Moy L, Kahn CE. Checklist for artificial intelligence in medical imaging (CLAIM): a guide for authors and reviewers. *Radiol Artif Intell*. 2020;2:e200029. https://doi.org/10.1148/ryai.2020200029
27. Tu J, Shen C, Liu J, et al. Detection of microscopic glioblastoma infiltration in peritumoral edema using interactive deep learning with DTI biomarkers: testing via stereotactic biopsy. *J Magn Reson Imaging*. 2025;62:1802-1811. https://doi.org/10.1002/jmri.70058
28. Eidel O, Burth S, Neumann JO, et al. Tumor infiltration in enhancing and non-enhancing parts of glioblastoma: a correlation with histopathology. *PLoS One*. 2017;12:e0169292. https://doi.org/10.1371/journal.pone.0169292
29. He L, Zhang H, Li T, et al. Distinguishing tumor cell infiltration and vasogenic edema in the peritumoral region of glioblastoma at the voxel level via conventional MRI sequences. *Acad Radiol*. 2024;31:1082-1090. https://doi.org/10.1016/j.acra.2023.08.008
30. Cepeda S, Romero R, Luque L, et al. Deep learning-based postoperative glioblastoma segmentation and extent of resection evaluation: development, external validation, and model comparison. *Neurooncol Adv*. 2024;6:vdae199. https://doi.org/10.1093/noajnl/vdae199
31. Ellingson BM, Wen PY, Cloughesy TF. Modified criteria for radiographic response assessment in glioblastoma clinical trials. *Neurotherapeutics*. 2017;14:307-320. https://doi.org/10.1007/s13311-016-0507-6
32. Cepeda S, Esteban-Sinovas O, Luppino LT, et al. Radiomics-based quantification of tumor infiltration in the non-enhancing peritumoral region on postoperative MRI is associated with survival in glioblastoma. *Sci Rep*. 2025;15:43932. https://doi.org/10.1038/s41598-025-27711-5
33. Durst CR, Raghavan P, Shaffrey ME, et al. Multimodal MR imaging model to predict tumor infiltration in patients with gliomas. *Neuroradiology*. 2014;56:107-115. https://doi.org/10.1007/s00234-013-1308-9
34. Chang PD, Malone HR, Bowden SG, et al. A multiparametric model for mapping cellularity in glioblastoma using radiographically localized biopsies. *AJNR Am J Neuroradiol*. 2017;38:890-898. https://doi.org/10.3174/ajnr.A5112
35. Gaw N, Hawkins-Daarud A, Hu LS, et al. Integration of machine learning and mechanistic models accurately predicts variation in cell density of glioblastoma using multiparametric MRI. *Sci Rep*. 2019;9:10063. https://doi.org/10.1038/s41598-019-46296-4
36. Hu LS, Yoon H, Eschbacher JM, et al. Accurate patient-specific machine learning models of glioblastoma invasion using transfer learning. *AJNR Am J Neuroradiol*. 2019;40:418-425. https://doi.org/10.3174/ajnr.A5981ajnr;ajnr.A5981v1
37. Gómez-Mahiques M, Lopez-Mateu C, Gil-Terrón FJ, et al. Revealing the infiltration: prognostic value of automated segmentation of non-contrast-enhancing tumor in glioblastoma. *medRxiv*. 2025; https://doi.org/10.1101/2025.06.26.25327675
38. Juan-Albarracín J, Fuster-Garcia E, Pérez-Girbés A, et al. Glioblastoma: vascular habitats detected at preoperative dynamic susceptibility-weighted contrast-enhanced perfusion MR imaging predict survival. *Radiology*. 2018;287:944-954. https://doi.org/10.1148/radiol.2017170845
39. Bobholz SA, Lowman AK, Brehler M, et al. Radio-Pathomic maps of cell density identify brain tumor invasion beyond traditional MRI-defined margins. *AJNR Am J Neuroradiol*. 2022;43:682-688. https://doi.org/10.3174/ajnr.A7477

40. Bobholz SA, Lowman AK, Connelly JM, et al. Noninvasive autopsy-validated tumor probability maps identify glioma invasion beyond contrast enhancement. *Neurosurgery*. 2024;95:537-547. https://doi.org/10.1227/neu.0000000000002898

41. Nocera G, Sanvito F, Yao J, et al. Independent histological validation of MR-derived radio-pathomic maps of tumor cell density using image-guided biopsies in human brain tumors. *J Neurooncol*. 2025;175:111-122. https://doi.org/10.1007/s11060-025-05105-x

42. Darmanis S, Sloan SA, Croote D, et al. Single-Cell RNA-Seq analysis of infiltrating neoplastic cells at the migrating front of human glioblastoma. *Cell Rep*. 2017;21:1399-1410. https://doi.org/10.1016/j.celrep.2017.10.030

43. Wang L, Li X, Xu C, et al. Unveiling novel cell clusters and biomarkers in glioblastoma and its peritumoral microenvironment at the single-cell perspective. *J Transl Med*. 2024;22:551. https://doi.org/10.1186/s12967-024-05313-5

44. Inoue A, Ohnishi T, Nishikawa M, et al. Identification of CD44 as a reliable biomarker for glioblastoma invasion: based on magnetic resonance imaging and spectroscopic analysis of 5-aminolevulinic acid fluorescence. *Biomedicines*. 2023;11:2369. https://doi.org/10.3390/biomedicines11092369

45. Nimbalkar VP, Kruthika BS, Sravya P, et al. Differential gene expression in peritumoral brain zone of glioblastoma: role of SERPINA3 in promoting invasion, stemness and radioresistance of glioma cells and association with poor patient prognosis and recurrence. *J Neurooncol*. 2021;152:55-65. https://doi.org/10.1007/s11060-020-03685-4

46. Tataranu LG, Turliuc S, Rizea RE, et al. A synopsis of biomarkers in glioblastoma: past and present. *CIMB*. 2024;46:6903-6939. https://doi.org/10.3390/cimb46070412

47. Vanni A, Matani F, Bonaudo C, et al. 5-ALA assisted surgery of human glioblastoma samples reveals an enrichment of T cells expressing PD-1 and CD103 in the intermediate and marginal layers. *Eur J Immunol*. 2025;55:e51681. https://doi.org/10.1002/eji.202451681

48. Balcerak M, Weidner J, Karnakov P, et al. Individualizing glioma radiotherapy planning by optimization of a data and physics-informed discrete loss. *Nat Commun*. 2025;16:5982. https://doi.org/10.1038/s41467-025-60366-4

49. Lipková , JAngelikopoulos P, Wu, S, et al. Personalized radiotherapy design for glioblastoma: integrating mathematical tumor models, multimodal scans, and bayesian inference. *IEEE Trans Med Imaging*. 2019;38:1875-1884. https://doi.org/10.1109/TMI.2019.2902044

Neuro-Oncology 2026 28(8) 1999–2013
https://doi.org/10.1093/neuonc/noag088
Clinical Investigations